Nat. Hazards Earth Syst. Sci. Discuss., doi:10.5194/nhess-2016-196, 2016
Manuscript under review for journal Nat. Hazards Earth Syst. Sci.
Published: 20 June 2016

Natural Hazards and Earth System Sciences
Discussions

The catastrophic landfill flowslide at Hongao dumpsite on December 20, 2015 in Shenzhen, China

Qiang Xu[1], Dalei Peng[1], Weile Li[1], Xiujun Dong[1], Wei Hu[1], Minggao Tang[1], Fangzhou Liu[2*]

[1]State Key Laboratory of Geohazard Prevention and Geoenvironment Protection, Chengdu University of Technology, Chengdu 610059, China
[2]School of Civil and Environmental Engineering, Georgia Institute of Technology, Atlanta, GA, USA

Abstract A catastrophic flowslide occurred at Hongao dumpsite at approximately 11:40 AM on Dec 20, 2015, in Guangming New District of Shenzhen, China. The flowslide damaged 33 buildings and caused total death toll of ~~69 and 8 missing~~, with the absence of extreme weather condition and seismic activity. The slope failure was analyzed on the basis of multi-temporal remote sensing images, site investigation, *in-situ* tests, laboratory experiment, and numerical analysis. The preliminary results showed that the volume of the flowslide deposit was ~~2.32×10^6~~ m^3 and the volume of dumpsite filling was ~~6.27×10^6~~ m^3 at the time of the event, ~~which is three times larger than the maximum design capacity.~~ The flowslide had the characteristics of high travel speed and long run-out distance, of which the displaced material was primarily silty soil from nearby construction sites with high moisture content. The primary causes of the failure were concluded as follow: (1) The dumpsite stagnated groundwater flow in the study area, which resulted in the saturation of the waste filling and high pore water pressure due to the underlying impermeable granite stratum; (2) The accumulation rate and total volume of the waste filling was in exceedance of the design capacity. The slope failure may be ascribed to excess pore water pressure as liquefaction were observed at many locations and it is postulated that such phenomena was related to the surcharge loads imposed by the unregulated disposal activities.

Keywords Flowslide, Landslide, Municipal Solid Waste (MSW), Dumpsite, Quarry, Landfill

1 Introduction

Owing to the rapid population growth and industrialization, increase in the accumulation rate of municipal solid waste (MSW) poses challenges in MSW management and urban planning (Huang and Cheng 2016). Landfilling is the most common method of MSW disposal management (Brunner and Fellner 2007; Huang and Cheng 2016). Transformation of an abandoned quarry to a MSW dumpsite is a general approach as it conserves resources by reclaiming the quarry space and provides MSW storage solution (Zou 2016). The landfill slope stability is critical in MSW management, and therefore, the selection and design of landfills require engineering assessment on slope stability and environment impact (Zou 2016).

The porosity and moisture content of MSW is typically high in unregulated landfills due to inadequate drainage system. Therefore, the residual soils in MSW may exhibit fluid flow behave, i.e. flow slide, with extremely high mobility in the event of a slope failure (Dai et al 2016; Huang and Cheng 2016). Study on the landfill slope failure in MSW dumpsite can be found in previous literatures, of which 6 reported cases between 1993 and 2005 resulted in around 500 deaths and significant properties loss (Mitchell et al 1990; Kjeldsen and Fischer 1995; Kocasoy and Curi 1995; Eid et al 2000; Blight and Fourie 2005; Merry et al 2005; Yılmaz and Atmaca 2006; Blight 2008). The deadliest event in history killed 278 people in Manila, Philippines in 2000, and the second deadliest event buried 71 houses and killed 143 people on Feb 21, 2005 at Leuwigajah dumpsite near Bandung, Indonesia, (Lavigne et al 2014).

Shear strength of MSW is a function of various parameters, such as waste type and composition, disposal rate, moisture contents, overburden pressure, and compaction (Eid et al 2000; Huvaj-Sarihan and Stark 2008). The movement of waste avalanches are complex and still poorly known (Lavigne et al 2014) due to the lack of field monitoring data. The existing studies have focused on empirical methods (e.g. Blight and Fourie 2005; Srour 2011), laboratory experiment, and numerical analysis. An approach was presented to estimate the maximum flow velocity of MSW slope failure based on energy balance (Blight and Fourie 2005). The empirical-statistical method still has widespread use in practical applications, but the accuracy is often model dependent (Dai et al 2016; Huang and Cheng 2016). The mixture of peat, kaolinite, and quartz sand were used in laboratory tests to simulate MSW landslide, of which the results shown that, with

Nat. Hazards Earth Syst. Sci. Discuss., doi:10.5194/nhess-2016-196, 2016
Manuscript under review for journal Nat. Hazards Earth Syst. Sci.
Published: 20 June 2016

Natural Hazards and Earth System Sciences
Open Access
Discussions

increased moisture content of the MSW, the mobility increases while the maximum and final flow depth decrease (Dai et al 2016). Numerical simulation has been widely used in the landfill slope stability analysis (Chang 2002; Chang 2005; Chugh et al 2007; Chen and Yuan 2009; Huang et al 2013; Huang and Cheng 2016). The Smoothed Particle Hydrodynamics (SPH) method was used for run-out distance analysis of two typical landfill flow slides occurred in Sarajevo and Bandung (Huang and Cheng 2016).

A MSW slope failure occurred at Hongao dumpsite, Guangming New District of Shenzhen, China at 11:40 AM on Dec 20, 2015, which destroyed 33 buildings and accommodations in the adjacent industrial park, and resulted in death of ~~69 with 8 missing~~ as of Jan 12, 2016. No extreme weather conditions or seismic activity were reported at the time of the event. This article aims at investigating the characteristics and causes of the flowslide. Field investigation, *in-situ* test, UAV stereo-measurements, and remote sensing image interpretation were applied to recover material properties and landform characteristics of the study area. Laboratory experiment and numerical analysis were performed to improve understanding on the failure process.

2 Data and Methodology

2.1 Satellite Images, Topographic Map, and Aerial Photo

A series of high resolution satellite images was identified on Google Earth between Nov 2002 and Feb 2016. A Pleiades remote sensing image of the study area obtained on Dec 18, 2015 (2 days before the event) was used to facilitate the analysis (Fig. 1a). Topography map of the pre-disposal site was provided by the local government, and the drawing was submitted by a third-party consulting firm in Dec 2013. According to the project report, the designed waste filling storage of was ~~2×10^6~~ m^3 with 10 slope benches at a ratio of 1:2.5. Aerial photos with resolution of 5 cm were collected by an Unmanned Aerial Vehicle (UAV) 3 days after the flowslide (Fig. 1b). The Digital Orthoimage Map (DOM) and Digital Surface Model (DSM) were reconstructed from the aerial photos, and a topographic map for the post-sliding dumpsite was generated from the DSM at the scale of 1:1000. As shown in the Pleiades image taken (Fig. 1a), a structured terrain for vehicles was excavated for around the pre-sliding dumpsite consisting of 8 benches and 3 platforms. The topographic map for the pre-sliding dumpsite was derived by overlaying the image of the original, pre-sliding, and post-sliding slopes, which provided estimation on the volume and depth of the pre-/post-sliding landfill.

2.2 Field Investigation and *in-situ* Tests

The first field investigation was conducted on Dec 23, 2015 and second investigation was deployed between Jan 21 and Jan 25, 2016. Field investigations assessed the topographical, geological, and groundwater conditions. The density, moisture content, and permeability of the displaced material of the flowside was measured from *in-situ* tests. The material properties were used in the subsequent laboratory experiment and numerical analysis.

2.3 Laboratory Tests

Undisturbed and disturbed soil samples were obtained for laboratory tests, including weathered silty soil and waste filling from the dumpsite. Grain size analysis was conducted by using the wet sieve method with sieve sizes of 20, 10, 5, 2.0, 1, 0.5, 0.25, 0.10, 0.075, 0.025, 0.01, 0.005, 0.002, and 0.001 mm. The maximum dry density and optimum moisture content of the displaced material were determined from the standard laboratory compaction test. The shear strength parameters of the displaced material (c, Φ) were obtained by triaxial compression test.

2.4 Numerical Analysis

In order to analyze the stability of the dumpsite, input parameters for the material properties and model geometry were same as the corresponding values measured on site or in the laboratory. Factor of Safety (FOS) of the slope was calculated by using SLOPE/W software with Morgenstern Prince Limit Equilibrium Analysis method.

Nat. Hazards Earth Syst. Sci. Discuss., doi:10.5194/nhess-2016-196, 2016
Manuscript under review for journal Nat. Hazards Earth Syst. Sci.
Published: 20 June 2016

Natural Hazards and Earth System Sciences
Open Access
Discussions

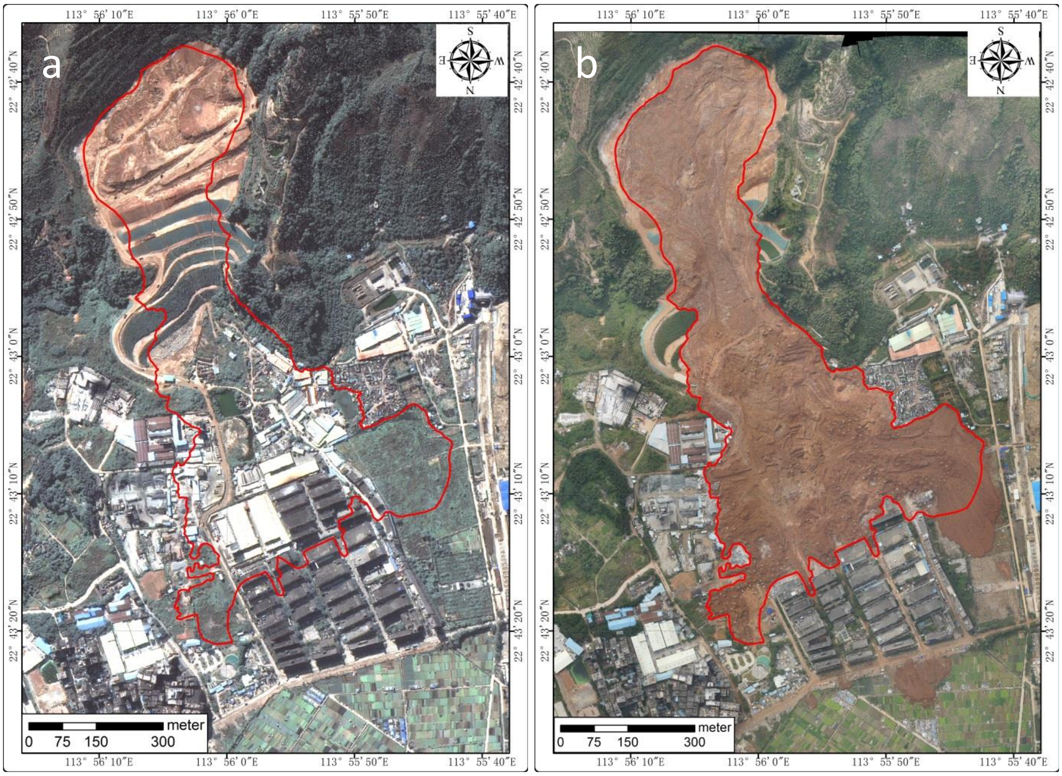

Fig. 1 Images for the Pre- and Post-sliding dumpsite. The boundary of the flowslide is indicated by the red line. **a** Pleiades satellite image (Dec 18, 2015); **b** Aerial photo (Dec 23, 2015).

3 Geological and Climatic Setting

The dumpsite is located at 23 km away from Shenzhen and 5 km away from the Guangming New District (E113°56'5", N22°42'44") as shown in Fig. 2. The dumpsite was surrounded by three ridges with a free face excavated with a mild slope gradient. The bedrock of the dumpsite is mainly Cretaceous granite rock (Fig. 3a, 3b, 3c, and 3d). The landfill consisted of construction waste with silty soil, clay, rock, and gravel (Fig. 3e and 3f).

The study area belongs to the zone of subtropical monsoon climate with an average temperature of 22° and an average annual precipitation of 1500 mm concentrating between April and September (greater than 85 % of the annual precipitation) (Zhang et al 2006). Based on the precipitation records from the nearby Tangjia Rainfall Station between Jan 1, 2013 and Dec 20, 2015 (Fig. 5), the accumulated precipitation in the study area was nearly 3240 mm, and field evidence suggested that the drainage facilities of the dumpsite were abandoned (Fig. 6b and 6c), which permits the ingress of rainwater in the quarry pit (Fig. 7c). The catchment area of the study area was 4.7×10^5 m^2, which was 2.95 times greater than the area of the dumpsite (1.6×10^5 m^2) as shown in Fig. 6a. Drainage system was implemented in the study area, where the surface run-off was designed to be collected by the drainage pipes installed at a higher elevation than the dumpsite and divert into the peripheral drainage channel. However, the drainage system failed to operate due to the absence of maintenance, and led to the concentration of surface run-off and groundwater into the dumpsite. Field test estimated that the permeability of the waste filling was 5.26×10^{-6} cm/s. Low permeability resulted in high moisture content and excess pore water pressure in the dumpsite. The groundwater in the study area ~~were~~ mainly bedrock fissure water and Quaternary pore water (Fig. 7).

Nat. Hazards Earth Syst. Sci. Discuss., doi:10.5194/nhess-2016-196, 2016
Manuscript under review for journal Nat. Hazards Earth Syst. Sci.
Published: 20 June 2016

Natural Hazards and Earth System Sciences
Discussions
Open Access

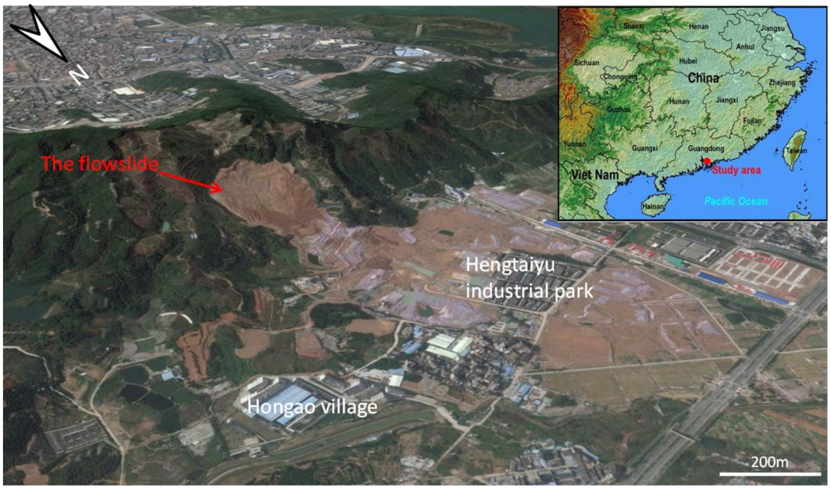

Fig. 2 Location of the study area and overview of the post-sliding dumpsite (Google Earth image taken on Feb 2016).

Fig. 3 Photos of the rock and soil specimen collected from the displaced material. **a** Exposed granite rock near the scarp of the landslide; **b** Close view of the granite rocks; **c** Drilling core samples; **d** Close view of the granite rock sample; **e** Displaced material in the zone of depletion; **f** Soils in the flowslide source area.

Nat. Hazards Earth Syst. Sci. Discuss., doi:10.5194/nhess-2016-196, 2016
Manuscript under review for journal Nat. Hazards Earth Syst. Sci.
Published: 20 June 2016

Natural Hazards and Earth System Sciences
Discussions
Open Access

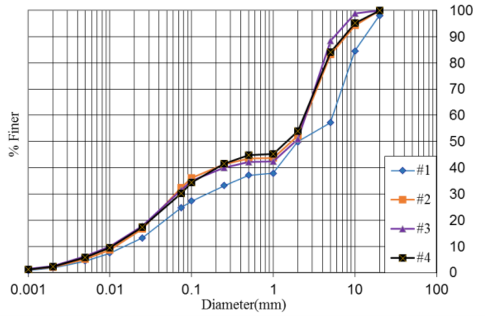

Fig. 4 Particle size distribution curves of the waste filling.

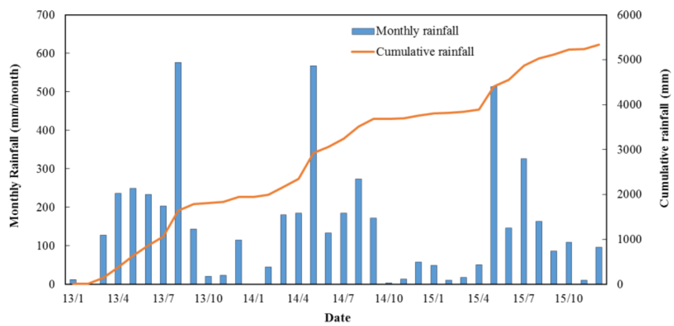

Fig.5 Monthly rainfall and cumulative precipitation between 2013 and Dec 2015.

Fig. 6 **a** An overview of the catchment area (Google Earth image); **b** The surrounding peripheral drainage channel of the dumpsite was abandoned; **c** Damaged drainage pipes were not repaired and failed to divert surface run-off into the peripheral drainage channel. Surface run-off concentrated in the waste filling.

Fig. 7 **a** Groundwater overflow in the rock fissures near the flowslide crown; **b** Water accumulation in the flowslide crown; **c** Surface run-off near the flowslide source area during rainfall event; **d** Eroded channel in dry condition; **e** Water accumulation in the source area; **f** Surface run-off and infiltration contributed to groundwater seepage.

4 Multi-Temporal Remote Sensing Images

The development and changes of the dumpsite is presented by multi-temporal remote sensing images taken between 2002 and 2016 (Fig. 8). It is postulated that the quarry was active between 2002 and 2008. However, formation of ponds of various sizes at different spatial and temporal locations in the quarry indicated low permeability and lack of drainage network (Fig. 8b, 8c, and 8d). The quarry was abandoned in or before 2008 as shown in Fig. 8c (obtained on 2/20/2008) with a small amount of waste filling in the quarry pit. A large-scale pond was formed due to groundwater and rainfall accumulation (Fig. 8d). The depth of the pit was over 100 m before the disposal activities. A service road was excavated between two rock hills exiting the quarry and formed a small-scale gully cross the pit longitudinally (Fig. 8a, 8b, 8c, and 8d). Additionally, a small-scale platform (abandoned office area of the quarry) was excavated at the immediate downstream of quarry exit. The gully was covered during construction of a multi-bench retaining slope between the rock hills as waste disposal continued throughout the process (Fig. 8e). Disposal activity was started around 2014 (Fig. 8e and 8f), and the accumulation rate of the waste filling was considerably fast (Zou 2016).

Nat. Hazards Earth Syst. Sci. Discuss., doi:10.5194/nhess-2016-196, 2016
Manuscript under review for journal Nat. Hazards Earth Syst. Sci.
Published: 20 June 2016

An unpaved road was excavated on the east of the quarry connecting the crest and toe of the hillslope as shown in Fig. 8e. A large number of trucks can be seen transporting waste filling to the dumpsite. A large amount of construction waste was dumped in the pit and four slope benches were built at the exit of the pit (Fig. 8e). The volume of the waste increased significantly with the first and second benches completed in late 2014, and the third to fifth benches were still under construction until Jan 2015 (Fig. 8f).

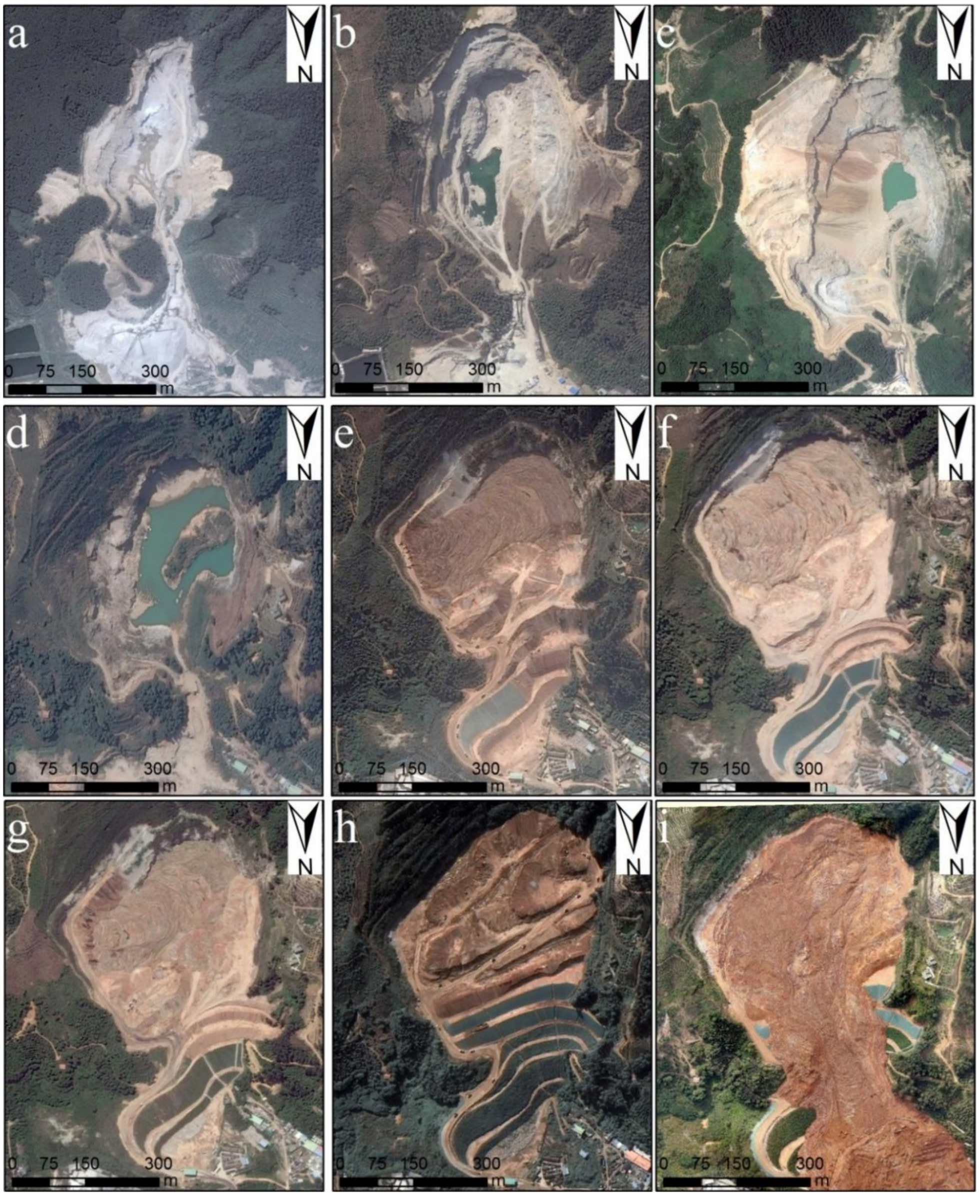

Fig. 8 Multi-temporal remote sensing images of the study area. **a** 08/31/2002; **b** 02/20/2008; **c** 08/30/2010; **d** 11/25/2013; **e** 11/17/2014; **f** 01/23/2015; **g** 04/14/2015; **h** Pleiades (12/18/2015); **f** Aerial (12/23/2015). Image **a** to **g** were obtained from Google Earth. A service road was excavated at the exit of the quarry with a width of nearly 70 m (see image **a**, **b**, **c**, and **d**).

Nat. Hazards Earth Syst. Sci. Discuss., doi:10.5194/nhess-2016-196, 2016
Manuscript under review for journal Nat. Hazards Earth Syst. Sci.
Published: 20 June 2016

Natural Hazards and Earth System Sciences
Open Access
Discussions

The rapid accumulation and total volume of the waste filling in the dumpsite gained some concerns before the flowslide. An environmental assessment provided by a third-party consulting firm warned the erosion at the site and its influence on the slope stability in Jan 2015 (Zou 2016). The disposal activity was ceased for a certain period as no trucks were seen in the daylight (Fig. 8f). The cease was verified by the interview with the local inhabitants. The disposal activity was resumed in or before April 2015, and the fourth bench was completed as shown in Fig. 8g. By comparing Fig. 8g and Fig. 8h, significant modifications on the landform can be seen in the study area with major increase in volume of the waste filling as the height of the landfill was close to the crest of the quarry pit. The waste filling was flattened and disposal activity was intense as more than 20 trucks appeared in Fig. 8h. Seven additional benches were completed with surface drainage channels installed on the hillslope, and the eighth bench was still under construction during the flowslide. The thickness of the dumpsite was estimated as 90 m with total volume of 6.3×10^{6} m^3 (Fig. 9a) by extracting the difference between the pre- and post-filling DEMs.

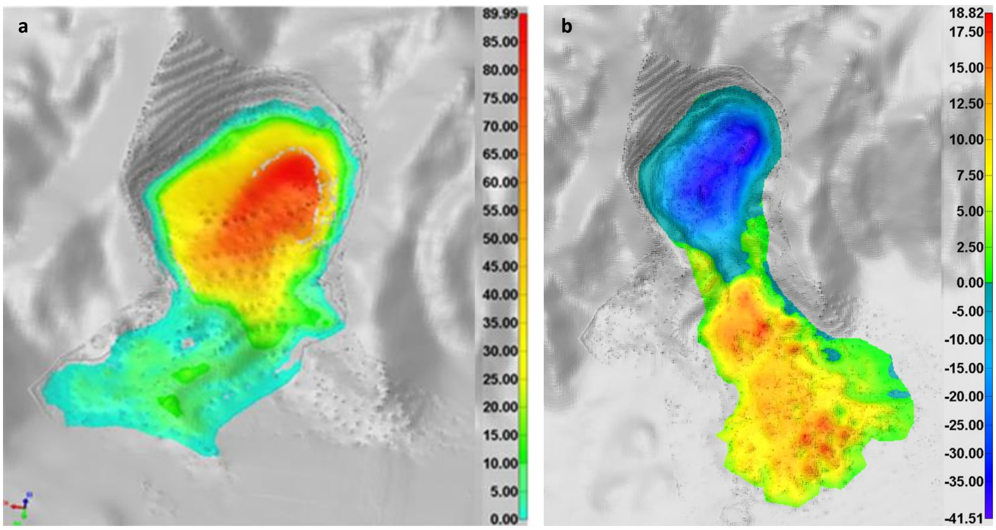

Fig. 9 **a** The thickness distribution of the dumpsite based on the pre-/post-disposal DEMs; **b** The elevation variations of the dumpsite estimated between the pre-/post-sliding DEMs.

5 Flowslide Characteristics

The flowslide area can be divided into the source area and flow-accumulation area as shown in Fig. 10. The source area was the pit of the abandoned quarry pit. The mass slid in the direction of nearly 340° with the maximum traveling distance of 1203 m. The maximum thickness of the remaining material in the source area was 41.51 m with an average of 20.5 m (Fig.11 and Fig. 12). The maximum deposit thickness in the flow-accumulation area was 18.2 m with an average of 8.21 m (Fig. 9b). The geometric characteristic of the flowslide can be expressed in length (L), height (H), width (W), and area (S) (Scheidegger 1973; Legros 2002). The geometric parameters are indicated in the simplified flowslide geometry in Fig. 13 with values listed in Table 1, Table 2 and Table 3.

Nat. Hazards Earth Syst. Sci. Discuss., doi:10.5194/nhess-2016-196, 2016
Manuscript under review for journal Nat. Hazards Earth Syst. Sci.
Published: 20 June 2016

Natural Hazards and Earth System Sciences
Open Access
Discussions

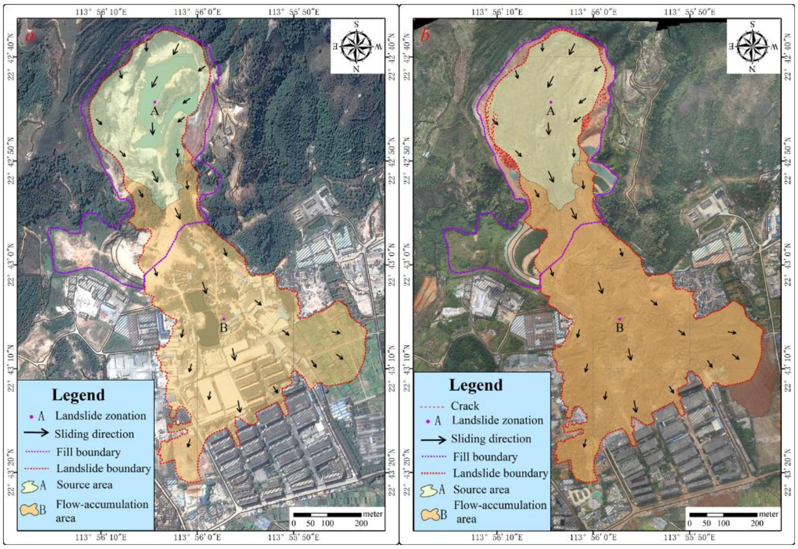

Fig.10 The direction of flowslide and distribution of the displaced material. **a** Flowslide overlying the pre-sliding industrial park showing the impact area and flow direction; **b** Aerial view of the flowslide.

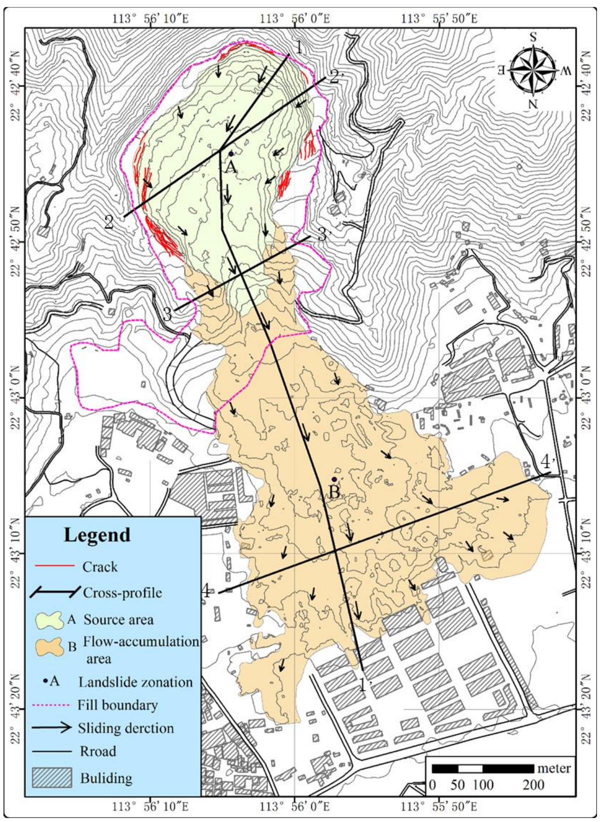

Fig.11 The topographic map of the flowslide.

Nat. Hazards Earth Syst. Sci. Discuss., doi:10.5194/nhess-2016-196, 2016
Manuscript under review for journal Nat. Hazards Earth Syst. Sci.
Published: 20 June 2016

Natural Hazards and Earth System Sciences
Discussions

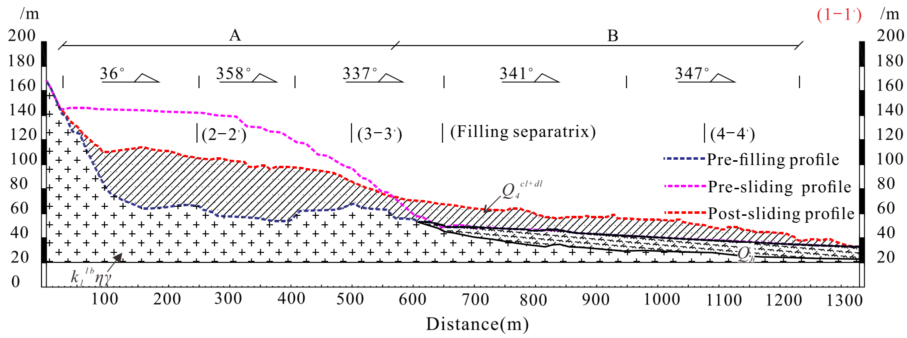

Fig.12 The geological and topographical cross section (profile line 1-1')

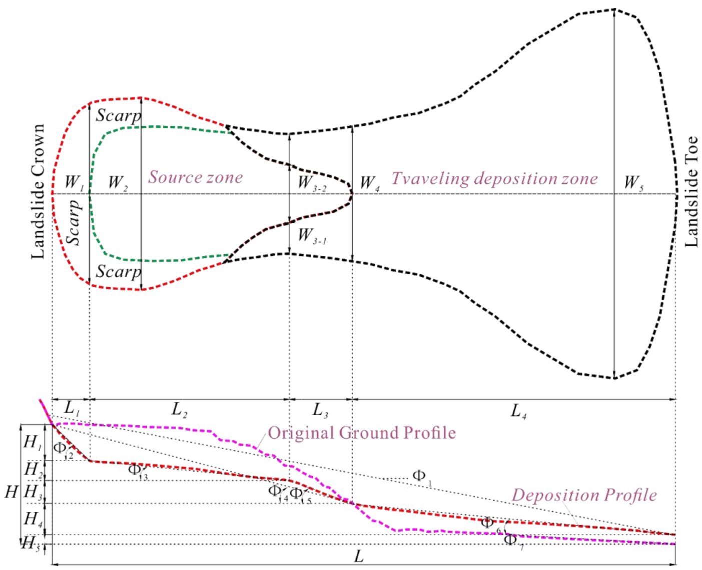

Fig. 13 Simplified illustration of the flowslide geometry. L: run-out distance; H: elevation; W_1: scarp width; W_2: max width of the source area; W_3: frontal width of the source area; W_4: width of the shear crack; W_5: max width of the flow-accumulation area; L_1: horizontal length of the scarp; L_2: horizontal length of the mild slope; L_3: horizontal length of the steep slope; L_4: horizontal length of the flow-accumulation area; H_1: height of the scarp; H_2: height of the mild slope; H_3: height of the steep slope; H_4: height of the flow-accumulation area; H_5: thickness of the toe of the flowslide; Φ_1: extension angle; Φ_2: slope gradient of the scarp; Φ_3: mild slope gradient; Φ_4: slope gradient of the source area; Φ_5: steep slope gradient; Φ_6: slope gradient of the flow-accumulation area; Φ_7: slope gradient of the foundation area

Table 1 Geometric parameters of the flowslide (Length and Width)

Parameter	L (m)	H (m)	W_1 (m)	W_2 (m)	W_{3-1} (m)	W_{3-2} (m)	W_{4-1} (m)	W_{4-2} (m)	W_5 (m)
Value	1204.67	111.31	212.5	399.32	218.31	149.38	217.71	64.63	592.25

Table 2 Geometric parameters of the flowslide (Angle)

Parameter	Φ_1 (°)	Φ_2 (°)	Φ_3 (°)	Φ_4 (°)	Φ_5 (°)	Φ_6 (°)	Φ_7 (°)	K	S (m^2)
Value	5.28	28.06	1.2	7.62	11.36	3.08	1.36	0.32	398619.6

Nat. Hazards Earth Syst. Sci. Discuss., doi:10.5194/nhess-2016-196, 2016
Manuscript under review for journal Nat. Hazards Earth Syst. Sci.
Published: 20 June 2016

Natural Hazards and Earth System Sciences
Open Access
Discussions

Table 3 Geometric parameters of the flowslide (Area and Thickness)

Parameter	Area A	Area B
S (m^2)	11.35×10^4	28.51×10^4
V (m^3)	2.32×10^6	2.34×10^6
T_{max} (m)	41.51	18.82
T_{ave} (m)	20.49	8.21

5.1 Source Area

The source area of the flowslide is the quarry pit with a length (L_{1+2+3}) of 540.30 m and a width (W_2) of 399.32 m. The area of the source area (S_A) is 11.35×10^4 m^2 and the height (H_{1+2+3}) was 68.5 m with an apparent dip (Φ_4) of 7.62° (Fig. 14 and Table 1). The volume of the mobilized material in the source area was 2.32×10^6 m^3 and the remained volume was 3.95×10^6 m^3. The maximum thickness of the source area ($T_{A\text{-}max}$) was 41.5 m with an average thickness ($T_{A\text{-}ave}$) of ~~20.5~~ m. The scarp located on the west of the main scarp has steep slope gradient with mild gradient on the east. The height of the steep scarp ranged from 25 to 47 m, whereas the height of the mild scarp ranged from 10 to 20 m. The geological cross section (profile line 2-2’) of the source area is shown in Fig. 14. The maximum thickness of the source area was 40.65 m with an average of 34.83 m. The overview of the source area is shown in Fig. 15, with details on the remaining material presented in Fig. 16.

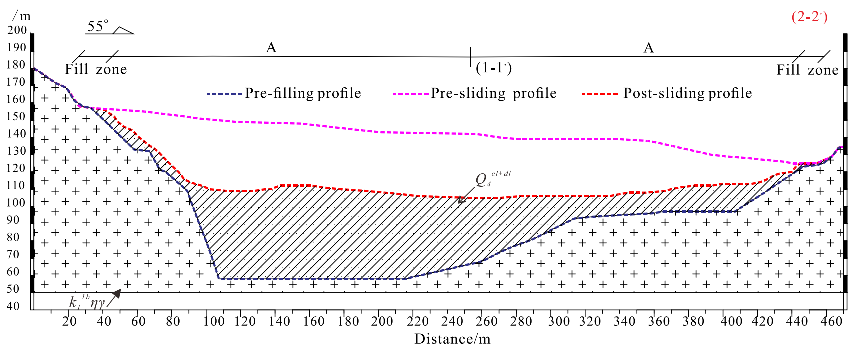

Fig.14 The geological cross section (profile line 2-2’) of the source area.

With the ingress of rainwater and groundwater in the dumpsite, pore water pressure increases due to the low permeability of the underlying granite in the Cretaceous system. It is appeared that the lack of drainage resulted in waste filling saturation in the lower portion of the dumpsite, which in turn formed the sliding bed of the flowslide (Fig. 15 and Fig. 16).

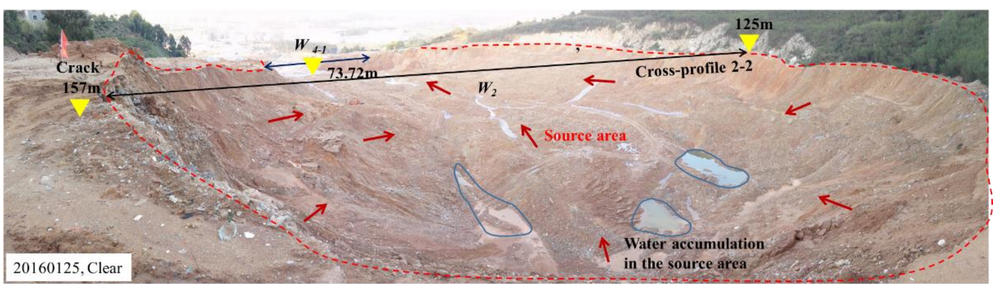

Fig.15 An overview of the source area (image taken at the flowslide crown facing north). A large opening ($W_{4\text{-}1}$) formed due to the failure of the retaining slope (the exit of the original quarry pit), which provided passage for the flowslide and permitted rapid release of kinematic energy.

Nat. Hazards Earth Syst. Sci. Discuss., doi:10.5194/nhess-2016-196, 2016
Manuscript under review for journal Nat. Hazards Earth Syst. Sci.
Published: 20 June 2016

Natural Hazards and Earth System Sciences Discussions

A large amount of silty soil were observed in the source area (Fig. 16). It is postulated that the material on both sides of the source area were mobilized due to the debuttressing effect as the waste filling in the lower portion of the dumpsite slid into the downstream industrial park, and in consequence, resulted in the collapse of the dumpsite. Step-like steep scarp was formed on the west part of the main scarp area (Fig. 17c and 17d), with tensile cracks developed on the rear edge as well as both sides of the scarp.

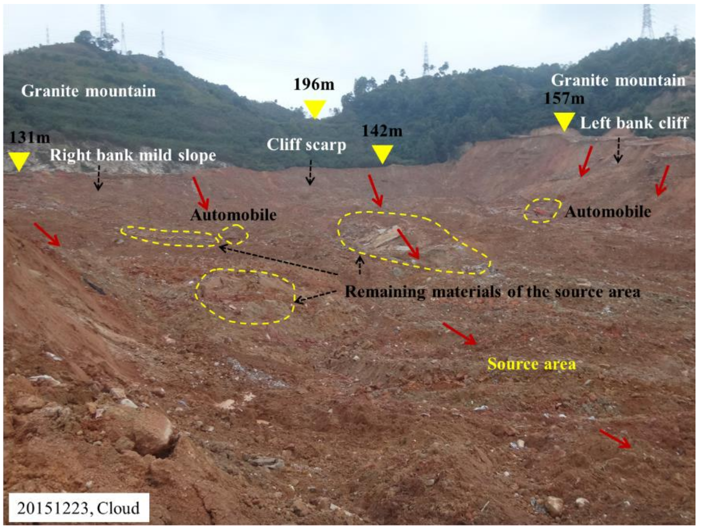

Fig.16 An overview of the remaining material in the source area (image taken near the quarry pit exit facing south). Several service vehicles parked in the rear edge of the dumpsite were dragged into the source area as waste filling slide into the industrial park. Blocky rock fragments were found in the source area.

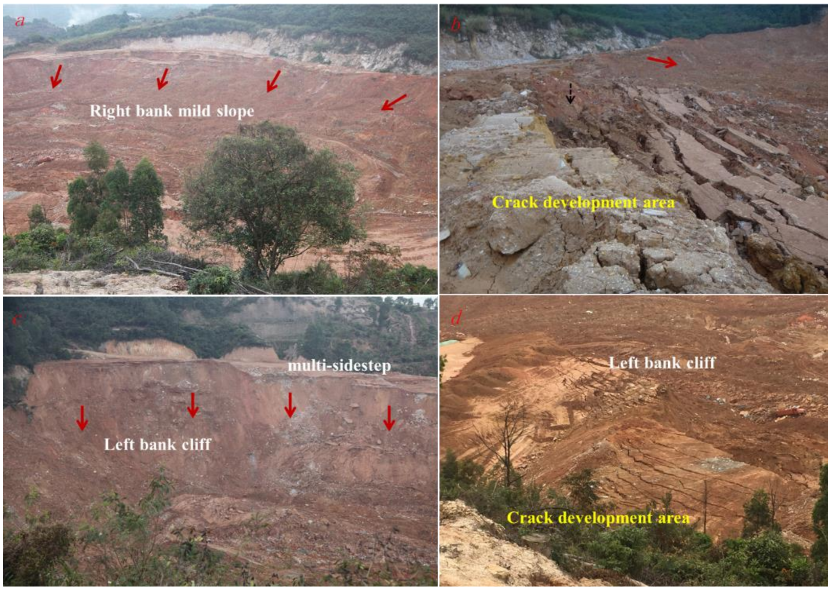

Fig.17 Characteristics of the remaining material in the source area. **a** Mild scarp on the east part of the main scarp area; **b** Cracks were developed in the west boundary of the flowslide; **c** Step-like steep scarp on the west part of the main scarp area; **d** An overview of the west part of the flowslide crown.

The presence of the aforementioned rock hills formed unfavorable topography for retaining slope stability by promoting a narrow gully for groundwater flow (Fig. 8c and Fig. 10b). As a result of the retaining slope failure, a large opening was formed at the elevaton of 73.7 m between the front edge of the steep scarp and the rear edge of the flow-accumulation area as shown in Fig. 11, Fig. 12, and Fig. 15. The displaced material was stratified in the middle part of the flow-accumulation area during the high speed sliding process. The shape of the failed retaining slope was half-elliptic-like with a width (W_{4-1}) of 217.7 m and a height (H_b) of 27.5 m (Fig. 18 and Fig. 19).

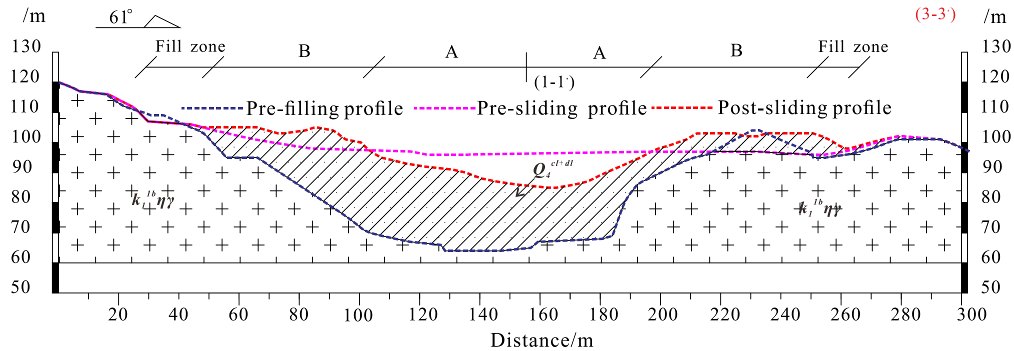

Fig. 18 Geological cross section (profile line 3-3') of the failed retaining slope located at the original quarry pit between the two rock hills.

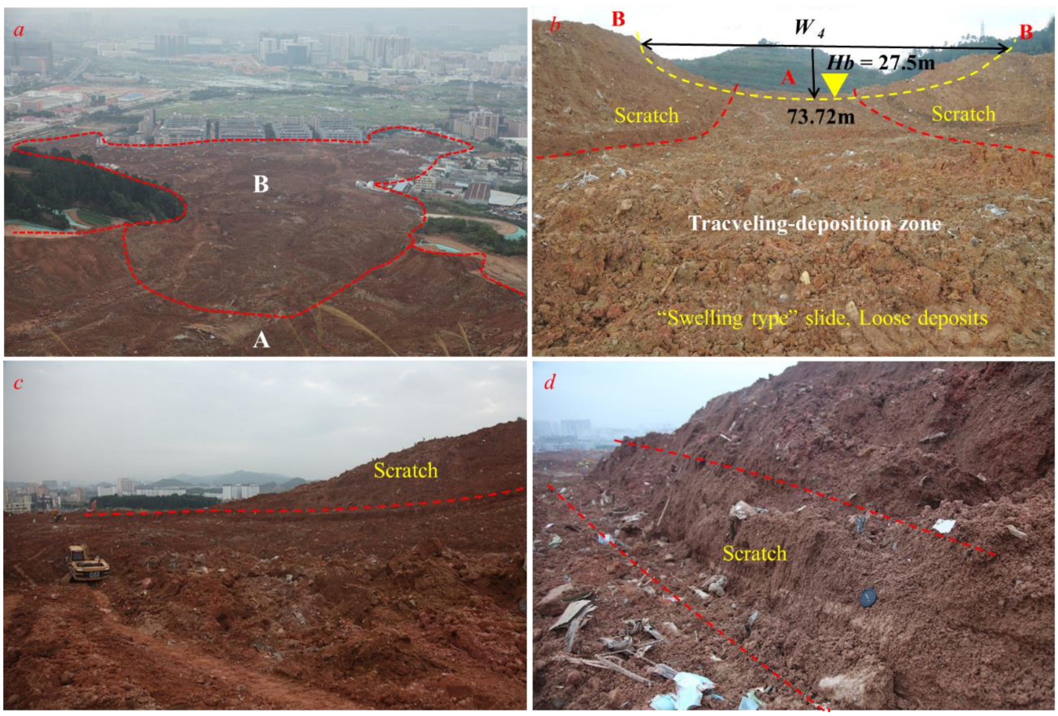

Fig. 19 **a** An overview of the exit of the flowslide between the source and flow-accumulation area (Photo courtesy of China News Agency); **b** The half-elliptic-like opening of the failed retaining slope; **c** East side of flow-accumulation area adjacent to the opening showing scratch caused by the flowslide; **d** Details on the scratches.

Nat. Hazards Earth Syst. Sci. Discuss., doi:10.5194/nhess-2016-196, 2016
Manuscript under review for journal Nat. Hazards Earth Syst. Sci.
Published: 20 June 2016

5.2 Flow-Accumulation Area

The fan-shaped flow-accumulation area mantled the retaining slope of the dumpsite and a large part of the industrial park ~~as~~ shown in Fig. 20. The original slope gradient of the industrial park (Φ) was 1.36° along the profile line 1-1' as shown in Fig. 14 and Table 1. The area immediately downstream of the landfill was relatively flat with no major construction except a pond (approx. 3600 m^2) and a channel (width: 7 m and length: 130 m). Most of the industrial structures were constructed on east, west, and north side of the pond as shown in Fig. 10a, and therefore, created a ideal flow channel for the mass movement. The failure of the rock retaining slope resulted in an opening for the waste fill flow and destoryed downstream bluildings (Fig. 20 and Fig. 21).

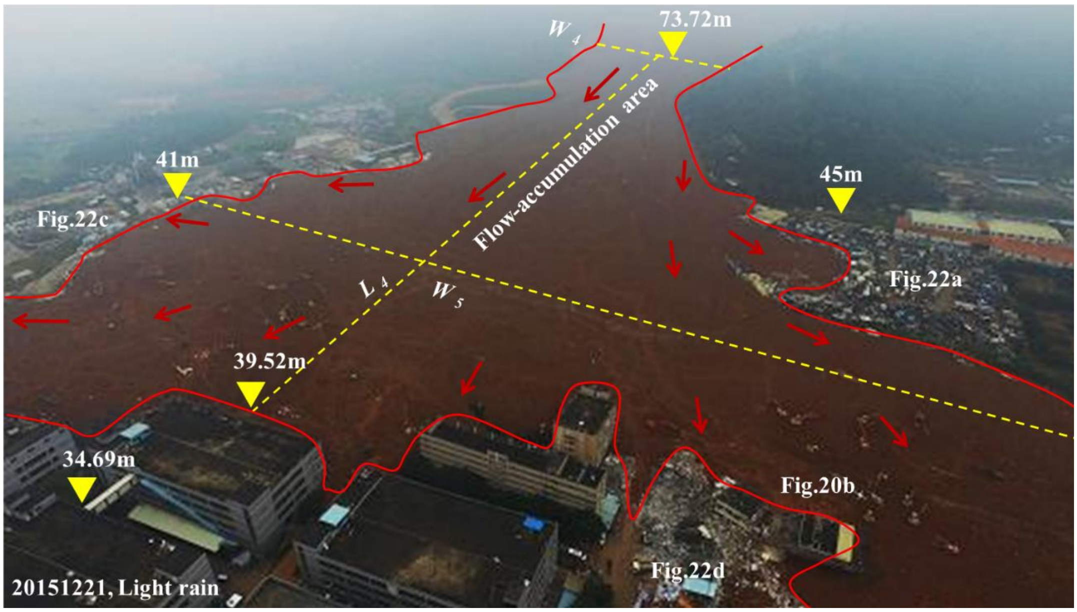

Fig. 20 The overview of the flow-accumulation area with elevations (Photo courtesy of China News Agency)

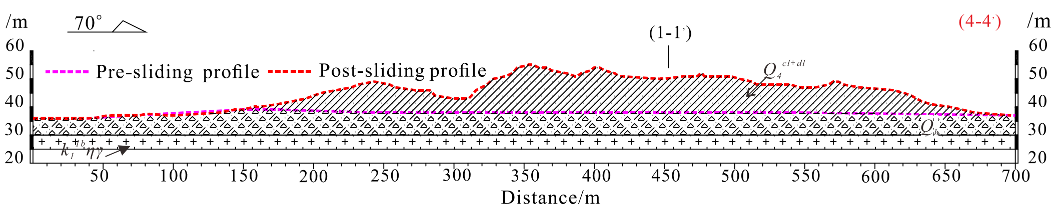

Fig. 21 Geological cross section (profile line 4-4') of the flow-accumulation area. The length (L_4) was 664.4 m and the width (W_3) was 218.3 m with the width of the front edge (W_5) of 592.3 m. The area of the flow-accumulation area is 28.51×10^4 m^2 and the elevation difference (H_4) was 35.7 m with the apparent dip (Φ_6) of 3.08°. The average thickness in the flow-accumulation area was 8.21 m with the maximum thickness of 18.82 m (Fig. 14, Table 1, and Table 3).

Nat. Hazards Earth Syst. Sci. Discuss., doi:10.5194/nhess-2016-196, 2016
Manuscript under review for journal Nat. Hazards Earth Syst. Sci.
Published: 20 June 2016

Natural Hazards and Earth System Sciences
Open Access
Discussions

Fig. 22 The damage of buildings in the industrial park (Photo courtesy of China News Agency).

5.3 Flowslide Movement

The source area of the flowslide was in the elevation of 142 m and the horizontal run-out distance (L) was approximately 1203 m, with the elevation difference (H) of 111 m. The sliding velocity can be estimated on the basis of the landslide geometrical characteristics. The velocity of the high-speed landslide can be estimated using the following expression (Scheidegger 1973):

$$\mathrm{v} = \sqrt{2g \times (\mathrm{H} - f \times \mathrm{L})} \tag{1}$$

Where v is the sliding velocity (m/s), g is the gravitational acceleration (m/s^2), H and L is the elevation difference and horizontal distance (m) between the crown and toe of the flowslide, respectively, and f is the equivalent friction coefficient referred as the ratio between the height and run-out distance of the flowslide (f = H/L). The equivalent friction coefficient of the dumpsite flowslide is 0.092. The relations of the run-out distance, elevation difference, and equivalent friction coefficient can be defined in light of the flowslide geomoetry (Fig. 13). The sliding velocity was calculated and presented in Fig. 23.

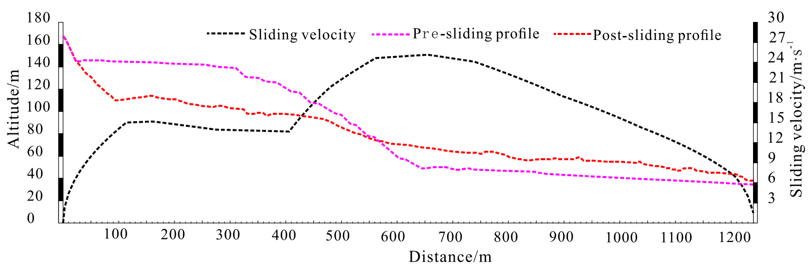

Fig. 23 The relationship between sliding velocity along profile line 1-1' and pre-/post-sliding landform.

Based on the calcuated sliding velocity profile, two sharp increases in the velocity can be seen, including the movement of the waste filling near the steep scarp and the acceleration of the flowslide exiting the pit. The sliding velocity of the mass accelerated to 15.17 m/s as waste filling reached the bottom of the steep scarp. The velocity displaced material gradually decreased to approximately 13 m/s before ~~accelerate~~ to the maximum velocity of 25.15 m/s as it reached ~~to~~ the opening of the dumpsite. The second sharp acceleration was followed by ripid dissipation of kneimatic energy and reduction on the velocity as it reached the flow-accumulation area (elev. 50 m). It was estimated that the sliding velocity was reduced to 15.68 m/s when it made contact with downstream buildings, and then ceased moving due to the obstruction of structures. The geometry and velocity exhibited the characteritics of high-speed long run-out flowslide.

6 Laboratory Experiment

Based on *in-situ* tests for waste filling density and moisture content as well as the laboratory compaction test, it was found that the dry density varies from 1.25 to 1.48 g/cm^3 and void ratio ranged between 0.83 and 1.31. Standard compaction test results suggested that the optimal water content of the waste filling was 15.31% with the highest dry density of 1.79 g/cm^3. The surface of the waste filling was in loose state with degree of compaction of the dumpsite ranged from 69.83% to 82.68%. Undrained shear test estimated that c and Φ of the waste filling is 4.7 kPa and 31.9°, respectively (Fig. 24), which is considerbly higher than gradient of the retaining slope.

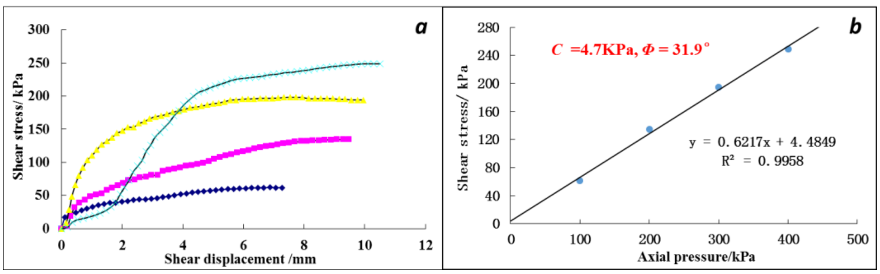

Fig. 24 Shear strength of the waste filling specimen obtained by undrained shear test.

7 Numerical Analysis

The numerical analysis aims at inverse analyzing the friction angle of the waste filling under the occurrence of the flowslide. Dumpsite slope ~~FoS~~ was estimated by using SLOPE/W software with Morgenstern Prince Limit Equilibrium Analysis method. Since ~~it~~ is postulated that the sliding mass in the lower portion of the dumpsite was saturated prior to the flowslide, a hypothetic sliding surface and the groundwater level were added into the model. The ~~FoS~~ was determined with an iterative approching by changing the postion of the sliding surface until failure of the dumpsite (Fig. 25 and Fig. 26). The physical parameters for the model were determined by the laboratory experiments and inversion analysis (Table 4).

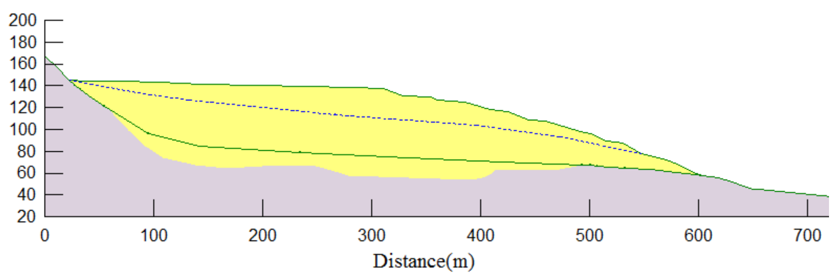

Fig. 25 Hypothetic sliding surface (green solid line) and groundwater level (blue dash line) in 2D numerical model.

add elevation(m)

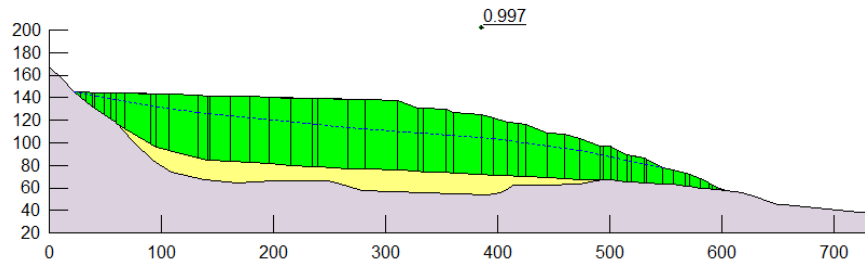

Fig. 26 Estimated ~~FoS~~ for the 2D numerical model.

Table 4 Material properties and parameters for the model

	Laboratory Experiment			Inversion Analysis		
	Unit Weight (kN/m^3)	c (kPa)	Φ (°)	Unit Weight (kN/m^3)	c (kPa)	Φ (°)
Waste Filling	16.5	-	-	16.5	-	-
Waste Surface	-	5	31	-	5	9.4

The results of slope stability analysis ~~is~~ presented in Table 5. Based on the numerical analysis, it was found possible for the development of a sliding surface above the bedrock in the lower portion of the waste filling. It is evident that the permeability of the waste filling was considerably low, which may result in saturation in the lower portion of the waste filling. As no clear drainage passage ~~were~~ found for the waste filling, the displaced material may remain undarined during the flowslide so that the shear strength was significantly reduced. The substaintial difference in the shear parameters obtained from laboratory test and numerical analysis indicated that the conventional numerical analysis is not appropriate for analyzing the failure mechanism of the flowslide. Additionally, the uncertainty of groundwater condition affects the analysis.

Table 5 Results of the numerical slope stability

Parameters	Unit Weight (kN/m^3)	c (kPa)	Φ (°)	FoS
Value	16.5	5	9.4	0.997

8 Discussion and Conclusion

The topography of the flowslide has the following features: (1) Suitable topography with a height of 124 m between the crown and toe of the flowslide ~~which~~ stored large potential energy needed for high speed and long run-out distance flowslide; (2) Low permeability of the waste filling in the dumpsite with impermeable bedrock resulted in groundwater stagnation. However, the failure of the retaining slope formed a narrow opening for the subsequent flowslide, with sudden release of high kinematic energy generating high sliding velocity and long travel distance.

Since the parameters obtained by the inversion analysis were largely different from the experimental results, it is postulated that the deformation and failure of the landfill was ascribed to the excess pore water pressure in the waste filling. The sharp increase of the pore water pressure causes significant destruction and results in liquefaction. Localized liquefactions were found at several locations on the study area (Fig. 27). The exact reason for the surge in the pore water pressure remains unclear at this point, however, it may involve: (1) rapid surcharge loading in the dumpsite while pore water pressure cannot dissipate immediately; (2) the waste filling was loosely packed with large pores in the microstructure, and the collapse of particle structure ~~lead~~ to the shrinkage of pores, and in turn ~~building~~ excess pore water pressure.

Nat. Hazards Earth Syst. Sci. Discuss., doi:10.5194/nhess-2016-196, 2016
Manuscript under review for journal Nat. Hazards Earth Syst. Sci.
Published: 20 June 2016

Fig. 27 Evidence of liquefaction near the opening of the failed retaining slope.

The engineering background of the dumpsite prior to the event include mainly three phases, i.e. the mining process of the quarry, construction of the downstream industrial zone, and waste filling process. However, the previous engineering undertakes posed very limited influence on the stability of site, and based on the field investigations, the volume of the waste filling was estimated as ~~6.27×10^6~~ m^3, which was three times larger than the design capacity of the dumpsite.

The dumpsite flowslide is divided into the source area and flow-accumuation area. The volume of the source area was 2.32×10^4 m^3 with the ~~max.~~ and average thickness of 41.5 m and 20.5 m, respectively. The volume of the fan-shaped flow-accumulating area was 2.34×10^6 m^3 with the max. and average thickness of 18.8 m and 8.2 m, respectively. The volume expansion coefficient of flowslide was 1.007. The ~~maximan~~ sliding velocity of the flowslide was 25.15 m/s at the opening of the dumpsit, and reduced to 15.68 m/s as it reached the industrial park and ceased moving due to the obstruction of buildings. The flowslide is charcteristiced by high speed and long run-out distance. The laboratory test and numerical model yielded largely different results for the shear strength of the waste filling. Meanwhile, field investigation indicated liquidation at several locations on the site. Unregularly disposal activites in addition to the ingress of rainwater and high pore water pressure played important roles in deformation process of the dumpsite. Although the flowslide destruction process was fast with excessive amount of waste filling accumulation, it is postulated that signs of deformation may have already appeared in the study site but not discovered due to the absence of field monitoring. Further analysis is undergoing at SKLGP to assess the causes ~~involoved~~ for generating the excess pore water pressure.

Acknowledgments The work is financially supported by the NSFC (Grant No. 41521002) and the National State Key 973 Project (Grant No. 2014CB744703) from the Ministry of Science and Technology of the People's Republic of China.

Reference

Blight G (2008) Slope failures in municipal solid waste dumps and landfills: a review. Waste Manag Res 26:448–463. doi: 10.1177/0734242X07087975

Nat. Hazards Earth Syst. Sci. Discuss., doi:10.5194/nhess-2016-196, 2016
Manuscript under review for journal Nat. Hazards Earth Syst. Sci.
Published: 20 June 2016

Blight GE, Fourie AB (2005) Catastrophe revisited–disastrous flow failures of mine and municipal solid waste. Geotech Geol Eng 23:219–248.

Brunner PH, Fellner J (2007) Setting priorities for waste management strategies in developing countries. Waste Manag Res 25:234–240. doi: 10.1177/0734242X07078296

Chang M (2002) A 3D slope stability analysis method assuming parallel lines of intersection and differential straining of block contacts. Can Geotech J 39:799–811. doi: 10.1139/t02-020

Chang M (2005) Three-dimensional stability analysis of the Kettleman Hills landfill slope failure based on observed sliding-block mechanism. Comput Geotech 32:587–599.

Chen Z, Yuan J (2009) An Extended Environmental Multimedia Modeling System (EEMMS) for Landfill Case Studies. Environ Forensics 10:336–346. doi: 10.1080/15275920903347396

Chugh AK, Stark TD, DeJong K a (2007) Reanalysis of a municipal landfill slope failure near Cincinnati, Ohio, USA. Can Geotech J 44:33–53. doi: 10.1139/t06-089

Dai Z, Huang Y, Jiang F, Huang M (2016) Modeling the flow behavior of a simulated municipal solid waste. Bull Eng Geol Environ 75:275–291. doi: 10.1007/s10064-015-0735-8

Daouadji A, Hicher P (2010) An enhanced constitutive model for crushable granular materials. Int J Numer Anal Methods Geomech 34:555–580.

Eid HT, Stark TD, Evans WD, Sherry PE (2000) Municipal solid waste slope failure. I: Waste and foundation soil properties. J Geotech Geoenvironmental Eng 126:397–407.

Huang Y, Cheng H (2016) A simplified analytical model for run-out prediction of flow slides in municipal solid waste landfills. Landslides (Published:1–9. doi: 10.1007/s10346-016-0688-4

Huang Y, Dai Z, Zhang W, Huang M (2013) SPH-based numerical simulations of flow slides in municipal solid waste landfills. Waste Manag Res 31:256–64. doi: 10.1177/0734242X12470205

Huvaj-Sarihan N, Stark TD (2008) Back-Analyses of Landfill Slope Failures. 6th Int Conf Case Hist Geotech Eng 1–7.

Kjeldsen P, Fischer E V (1995) Landfill gas migration - field investigations at Skellingsted landfill, Denmark. Waste Manag Res 13:467–484.

Kocasoy G, Curi K (1995) The Ümraniye-Hekimbaşi open dump accident. Waste Manag Res 13:305–314.

Lavigne F, Wassmer P, Gomez C, et al (2014) The 21 February 2005, catastrophic waste avalanche at Leuwigajah dumpsite, Bandung, Indonesia. Geoenvironmental Disasters 1:1–12. doi: 10.1186/s40677-014-0010-5

Legros F (2002) The mobility of long-runout landslides. Eng Geol 63:301–331.

Merry SM, Kavazanjian Jr E, Fritz WU (2005) Reconnaissance of the July 10, 2000, Payatas landfill failure. J Perform Constr Facil 19:100–107.

Mitchell JK, Seed RB, Seed HB (1990) Kettleman Hills waste landfill slope failure. I: Liner-system properties. J Geotech Eng 116:647–668. doi: 10.1061/(ASCE)0733-9410(1990)116:4(647)

Nicot F, Darve F (2011) Diffuse and localized failure modes: two competing mechanisms. Int J Numer Anal Methods Geomech 35:586–601.

Scheidegger AE (1973) On the prediction of the reach and velocity of catastrophic landslides. Rock Mech Rock Eng 5:231–236. doi: 10.1007/BF01301796

Srour G (2011) Mine waste failure: an analysis of empirical and graphical runout prediction methods. University of British Columbia

Yılmaz A, Atmaca E (2006) Environmental geological assessment of a solid waste disposal site: a case study in Sivas, Turkey. Environ Geol 50:677–689.

Zhang Y, Qi M, Ma H (2006) Slope instability and its control in Shenzhen City. Chinese J Rock Mech Eng S2 (in Chinese).

Zhao C, Dai F (2007) Study on failure mechanism of a fill slope in Shenzhen. Chinese J Geol Hazard Control 18:3412–3421 (in Chinese).

Zou DH (2016) Exploring a Waste Dump Site Failure–Possible Causes and Prevention Measures. Int J Geohazards Environ 2:25–33.